Materials Science and Engineering C 33 (2013) 298–303

Contents lists available at SciVerse ScienceDirect

Materials Science and Engineering C

journal homepage: www.elsevier.com/locate/msec

Comparative study of conductometric glucose biosensor based on gold and on magnetic nanoparticles

Wided Nouira [a,b,*], Abderrazak Maaref [b], Hamid Elaissari [c], Francis Vocanson [d], Maryam Siadat [e], Nicole Jaffrezic-Renault [a,**]

[a] Université de Lyon, Institut des Sciences Analytiques: Université Claude Bernard, Lyon 1, 43 Boulevard du 11 Novembre 1918, 69622 Villeurbanne, France
[b] Laboratoire des Interfaces et Matériaux Avancés, Université de Monastir, Avenue de l'Environnement, 5019 Monastir, Tunisia
[c] Université de Lyon, Laboratoire LAGEP CPE-308G: Université Claude Bernard Lyon-1, 69622 Villeurbanne Cedex, France
[d] Université de Lyon, Laboratoire Hubert Curien, Université de Saint-Etienne Jean-Monnet, F-42023 Saint-Etienne, France
[e] LASC, ISEA, Université de Metz, 7 rue Marconi, 57070 Metz, France

ARTICLE INFO

Article history:
Received 7 March 2012
Received in revised form 27 July 2012
Accepted 29 August 2012
Available online 11 September 2012

Keywords:
Magnetic nanoparticles
Gold nanoparticles
Conductometric biosensor
Polyelectrolyte
Glucose oxidase

ABSTRACT

The aim of this study was to show the feasibility and the performances of nanoparticle biosensing. A glucose conductometric biosensor was developed using two types of nanoparticles (gold and magnetic), glucose oxidase (GOD) being adsorbed on PAH (poly(allylamine hydrochloride)) modified nanoparticles, deposited on a planar interdigitated electrode (IDEs). The best sensitivities for glucose detection were obtained with magnetic nanoparticles (70 μM/mM and 3 μM of detection limit) compared to 45 μM/mM and 9 μM with gold nanoparticles and 30 μM/mM and 50 μM with GOD directly cross-linked on IDEs. When stored in phosphate buffer (20 mM, pH 7.3) at 4 °C, the biosensor showed good stability for more than 12 days.

1. Introduction

The branch of science at the interface of physics, chemistry, materials science, and molecular biology referred to as nanotechnology has been intensively developed in the past 10–15 years. Nanotechnology (NT) has revolutionized the industrial and market sectors with a great variety of products [1]. The use of nanomaterials (conducting polymer nanowires, carbon nanotubes, nanoparticles) for the design of biosensing devices constitutes an exciting and recent approach to improve the performance of detection platforms. The extremely promising prospects of nanomaterials are due to their unique properties.

Different nanoparticles (NP) are produced in the form of metals, metal oxides, semiconductors, polymers, carbon materials, organics or biological, and these exhibit morphological forms such as spheres, cylinders, disks, platelets, hollow spheres and tubes. In terms of size, nanoparticles occupy a boundary position between microcosm and macrocosm: they are much larger than ordinary molecules or ions, but much smaller than physical bodies. By nanoparticles are implied objects of all three dimensions of which lie in the range 1–100 nm, mainly 1–10 nm. These can be either individual particles or particle agglomerates [2].

The use of NPs in biosensors is a relatively new area of research. Nevertheless, literature already shows numerous examples of incorporating NPs into biodevices [3–7]. So far, there are nanobiosensors for the specific detection of biologically-relevant molecules (nucleic acids [8], proteins [9] and enzymes [10]) and sometimes for the detection of infectious agents [11]. Therefore, many efforts have been done for the application of magnetic NPs in immunoanalysis, immobilization, and purification of enzymes, DNA and protein, and anti-tumor drug transportation [12–14]. Furthermore, considerable effort has been devoted to the study of gold nanoparticles with variable size and shape due to their unique geometry-dependent optical, electronic, and catalytic properties in electronics and optics [15–19], particularly in the fields of biotechnology and nanotechnology [20–22].

The immobilization of an enzyme is an important feature in designing the biorecognition part of enzyme based biosensors. Many comprehensive reviews have been written on enzyme immobilization using nanoparticles thus reporting thousands of protocols [23–27]. A wide variety of methods have been employed in the immobilization of enzymes using, such as adsorption [28], entrapment [29], cross-linking [30], covalent attachment [31] and Langmuir–Blodgett (LB) technique [32,33]. Among these immobilization techniques, adsorption is the most general, easiest to perform and oldest physical immobilization method [34]. One among the enzymes, glucose oxidase can be immobilized onto

* Correspondence to: W. Nouira, Laboratoire des Interfaces et Matériaux Avancés, Faculté des Sciences de Monastir, Avenue de l'Environnement, 5019 Monastir, Tunisia.
** Corresponding author.
E-mail addresses: widednouira@yahoo.fr (W. Nouira), nicole.jaffrezic@univ-lyon1.fr (N. Jaffrezic-Renault).

0928-4931/$ – see front matter © 2012 Elsevier B.V. All rights reserved.
http://dx.doi.org/10.1016/j.msec.2012.08.043

the electrode by physical adsorption [35], ionic and covalent bonding [36–39], cross-linking [40], and entrapment [41,42]. The sequential adsorption of oppositely charged ions by layer-by-layer (LBL) self-assembly is an effective method to prepare multilayer thin films with controlled thickness, unique mechanical properties, and ordered molecules [43].

In conductometric enzymatic biosensors, enzymatic reaction is confined close to the interdigitated electrode surface, because enzyme is cross-linked in contact with this surface, in the presence or in the absence of nanoparticles. The interdigitated electrodes allow the measurement of the change of conductivity in the region defined by field lines. The involved thickness is of the order of the interdigit distance (few tens of μm) [44]. As it has been modeled [45,46], the observed steady-state response of the conductometric biosensor is the result of the reaction rate limited kinetics of the enzymatic reaction and the diffusive flux of enzymatic reaction products away from the transducer surface, in the boundary layer. The most detectable result of enzymatic reaction is pH variation; a pH limit value is reached at the transducer surface.

The example of glucose detection will be studied in this work. The resulting conductivity changes are produced by enzymatically catalysed oxidation of the substrate according to the following reaction [47]:

$$\text{Glucose} + O_2 + H_2O + \text{GOD} \rightarrow \text{Gluconolactone} \rightarrow \text{Gluconic acid} + H_2O_2.$$

The effect of buffer capacity is very high, as it has been shown in a previous paper [48]. It was then shown that an additional membrane on top of the enzymatic part can screen partly the effect of buffer capacity of the measuring medium by limiting the diffusion of buffer ions towards the enzymatic part.

This paper is devoted to elaborate and characterize a glucose biosensor using two types of nanoparticles (gold and magnetic nanoparticles). The enzyme immobilization on nanoparticle surface will allow a higher surface density of immobilized enzyme due to the high surface on volume ratio. Moreover, in the case of urease applied to urea detection a higher sensitivity was observed in the case of gold nanoparticles which was attributable to their high conductivity and their behavior as nanoelectrodes [49].

2. Experimental

2.1. Chemicals and apparatus

The following chemicals were used without further purification: the polyelectrolyte used in this study, poly(allylamine hydrochloride) (PAH) in water was purchased from Sigma-Aldrich. Bovine serum albumin (BSA), glutaraldehyde (GA) (grade II, 25% aqueous solution), NaH_2PO_4 (>99%) and $Na_2HPO_4 \cdot 12H_2O$ (>99%), glucose oxidase (GOx, from *Aspergillus niger*) were obtained from Sigma-Aldrich. Gold nanoparticles (size 23 nm) were made up and stored in clean glass vials. Chemicals (tetrachloroauric(III) acid trihydrate and sodium citrate dehydrate) used were of highest available purity and were supplied by Aldrich, Fluka and Sigma. Carboxyl-Adembeads (from Ademtech, Pessac, France) were monodispersed (diameter 200 nm) and these super-paramagnetic beads were composed of magnetic core (iron oxide content of about 70%) encapsulated by a highly cross-linked hydrophilic polymer shell with carboxylic groups. Stock concentrated solutions of glucose were prepared in 5 mM phosphate buffer solution (pH 7.3) and stored at 4 °C. All aqueous solutions were prepared using 18 MΩ·cm ultrapure water, obtained from a Millipore Milli-Q system.

2.2. Preparation of PAH-coated gold nanoparticles (PAH/AuNPs)

Gold nanoparticles were synthetized according to the following procedure: in a round flask of 0.1 L equipped with a condenser, 11.6 mg (2.9×10^{-5} mol) of tetrachloroauric(III) acid trihydrate were dissolved in 21 mL of pure water. Then this solution was heated to reflux. In another 0.1 L round flask, 27.4 mg (9.3×10^{-5} mol) of sodium citrate dihydrate was dissolved in 7 mL of pure water and then added to the first flask. During the addition the yellow gold chloride solution turned red indicating the formation of gold clusters. The mix was moderately stirred, refluxed during 30 min and was cooled to room temperature under continuous stirring to yield the nanoparticle solution. The laser granulometer measurement shows the absence of aggregates and a size of the nanoparticles of around 23 nm with a standard deviation of 5 nm. The plasmon band is around 527 nm.

A suspension of gold nanoparticles (1% w/w) was firstly centrifuged at 20 °C using a centrifugator 2–6 K SIGMA from Fisher Bioblock Scientific at 9000 g for 20 min. The rich supernatant phase was then eliminated and the gold nanoparticles were immersed in 100 μL of aqueous solutions of 5 mg mL^{-1} of PAH (positive charge), under mechanical stirring for 15 min [50]. After the adsorption process, PAH-coated gold nanoparticles were removed by similar centrifugation and redispersion in 20 mM of phosphate buffer at pH 7.3.

2.3. Coating of magnetic nanoparticles (MNPs)

1/500 of nanoparticles (suspension 3.03 %) was first homogenized under mechanical stirring for 15 min in 100 μL of ultrapure water, twice. The nanoparticles were then coated with an initial layer of PAH (positive charge), this step was performed in 100 μL of aqueous solutions of 5 mg/mL of PAH, under similar stirring conditions during 15 min. The nanobeads were then recovered by applying a mild magnetic field. The PAH rich supernatant phase was then eliminated and the nanoparticles were rinsed twice with ultrapure water under mechanical stirring during 10 min, and separated again under a mild magnetic field.

2.4. Enzyme immobilization

The PAH-coated gold nanoparticles and PAH-coated magnetic nanoparticles were dispersed in 20 mM phosphate buffer (pH 7.3) containing 6% of BSA, 4% of GOD and 10% of glycerol, as optimized in our previous work [50]. After 1 h of mixing, these solutions were centrifuged (for gold nanoparticles) or decanted under magnetic field (for magnetic nanoparticles) in the same conditions as described before and redispersed in 20 mM phosphate buffer. 0.2 μL of these solutions was deposited onto the sensitive area of the working sensor (Fig. 1). For preparation of the reference sensor, PAH-coated gold nanoparticles and PAH-coated magnetic nanoparticles were dispersed in 20 mM phosphate buffer (pH 7.3) containing 10% of BSA and 10% of glycerol. After separation and redispersion in 20 mM phosphate buffer, 0.2 μl of these solutions was deposited onto the sensitive area of the reference sensor. The sensors were then placed in saturated GA vapor for 30 min. After exposure, the biosensors were dried at room temperature for 15–30 min and stored at 4 °C before the experiments.

2.5. Control of biocoating through measurements of zeta potential

To control the final surface composition of PAH/NPs, the zeta potential of polyelectrolyte/NPs was measured as a function of pH using dynamic light scattering (DLS) by a Zetasizer Nano-ZS (Malvern Instruments). Measurements were performed at very low ionic strength (10^{-3} M NaCl).

2.6. Transmission electron microscopy measurements (TEM)

Transmission electron microscopy (TEM) images were obtained with a Phillips CM120 electron microscope (CMEABG, University of Claude Bernard Lyon I-France). One drop of highly diluted dispersion was placed onto a copper grid (mesh 200 and covered with formvar-carbon) and

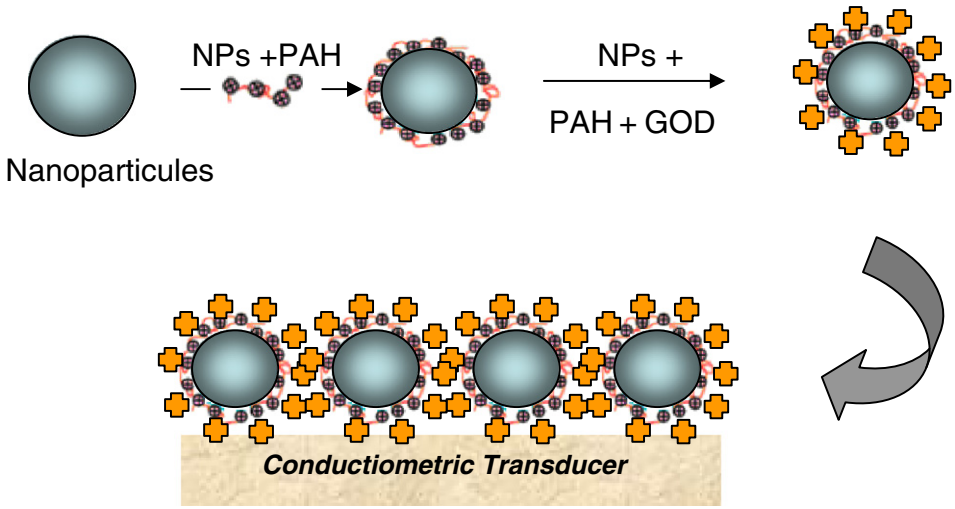

Fig. 1. Schema of principle of biosensor for glucose detection.

dried at room temperature before TEM analysis. The images were registered at 100 kV.

2.7. Conductometric measurements

The conductometric transducers, consisting of two identical pairs of gold interdigitated thin film electrodes (thickness: 150 nm), were fabricated by vacuum deposition on a ceramic substrate (5×30 mm) at the Lashkaryov Institute of Semiconductor Physics (Kiev, Ukraine). A 50 nm-thick intermediate chromium layer was used for better gold adhesion. The dimension of each interdigital space and digit was 20 μm and the length of the digits was about 1.0 mm. The sensitive area of each pair of electrodes was about 1 mm^2 [51]. Microelectrodes were placed in a glass cell filled with 5 mL of a 5 mM phosphate buffer pH 7.3. The solution was stirred vigorously. Measurements were then performed at 23 ± 2 °C by applying to the differential pairs of electrodes with an alternating voltage (10 mV amplitude, 100 kHz frequency) generated by a low-frequency wave-form generator (SR830 Lock-in amplifier from Stanford Research Systems). These conditions allowed reducing Faradaic processes, double-layer charging and concentration polarization at the microelectrode surface. After stabilization of the differential output signal, small aliquots (3–50 μL) of a concentrated substrate solution were added.

3. Results and discussion

3.1. Characterization of PAH-coated nanoparticles

3.1.1. Electrophoretic mobility measurements

Electrophoretic mobility measurements of particles dispersion are carried out as a function of pH at 25 °C in 10^{-3} mol/L NaCl solution. Each reported value is the average of five measurements. Electrophoretic mobility is converted into zeta potential by using Smoluchowski's equation [52]

$$\mu_e = \frac{\varepsilon}{4\pi\eta}\zeta$$

where μ_e is the electrophoretic mobility ($m^2\ V^{-1}\ s^{-1}$), ε is the dielectric constant, η is the viscosity of the medium (N s/m^2), and ζ is the zeta potential (mV).

The deduced zeta potential from the measured electrophoretic mobility was found to be negative irrespective of pH, which reveals the negative surface charge density of the particles. Below pH 6, the zeta potential increases in absolute value before reaching a plateau value of −30 mV above pH 6 (Fig. S1a). Such behaviour can be attributed to the presence of citrate groups on the AuNP surface, the higher pKa of citric acid being 6.4.

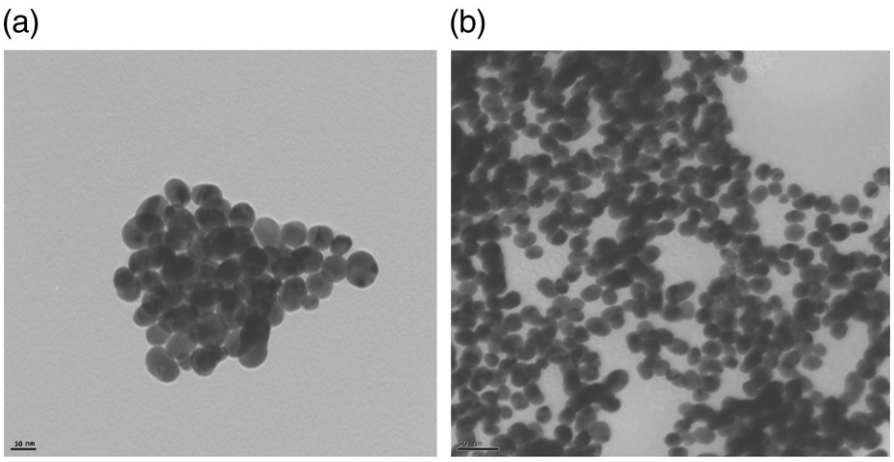

Fig. 2. TEM images of gold nanoparticles without (a) and with (b) PAH/GOD. Inserted bar represents 50 nm.

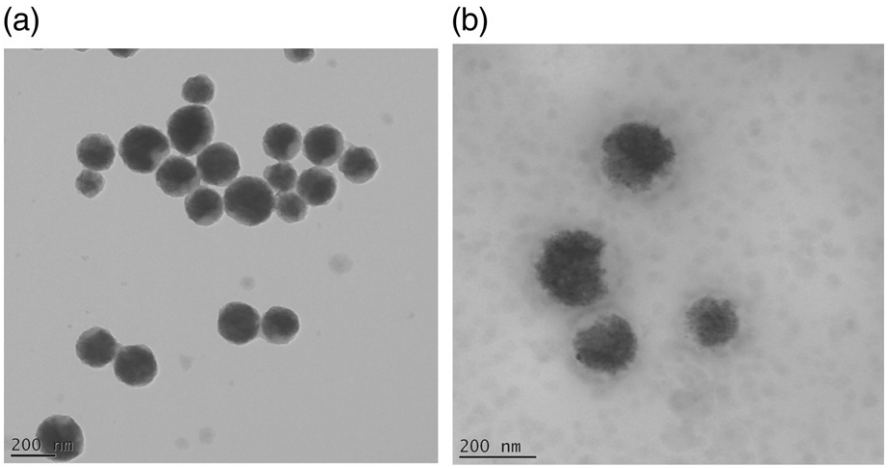

Fig. 3. TEM images of magnetic nanoparticles without (a) and with (b) PAH/GOD.

The zeta potential of coated gold nanoparticles with polyallylamine hydrochloride (PAH) was investigated as a function of pH (Fig. S1b). The zeta potential was found to be positive until pH 9.5. This positive character of the obtained particles can be attributed to the presence of cationic groups originated from the protonated amine function of PAH. In fact below pH 9.5, primary amine groups of PAH are protonated leading to cationic character. Whereas at pH 9.5 which correspond to the pKa of primary amine groups, the zeta potential was found to be zero corresponding to the isoelectric point of the obtained particles. Above pH 9.5, the observed negative zeta potential can be attributed to the OH^- condensation in the vicinity of the particles surface. The same result was observed for PAH/MNPs (not shown here).

3.1.2. TEM measurements

TEM analysis of gold nanoparticles revealed the polydispersity of the particles and also the spherical shape of the majority of the particles. In addition, the seed particles or the PAH containing gold particles exhibit the presence of some heterogeneity in chemical composition as clearly observed on TEM images (Fig. 2). In fact, the internal morphology of these gold nanoparticles exhibits the presence of two phases: one organic (transparent) and the second black part can be attributed to the inorganic gold part.

The PAH polymer cannot be clearly observed on the particles probably due to its low electronic density.

The observed TEM images of the manufactured magnetic latex particles revealed first the polydispersity character of the dispersion. The particles are spherical in shape and exhibit almost slight core-shell like morphology with magnetic core and polymer shell (Fig. 3).

3.2. Conductometric biosensor response

3.2.1. Analytical characteristics of glucose conductometric sensor using gold nanoparticles (GNPs)

Fig. 4 shows the steady-state response of the conductometric biosensor after glucose addition. It appears that the higher conductance response of the biosensors was 49 μS for 1 mM glucose concentration.

In order to investigate the effect of GNPs on the amplitude of response of the glucose biosensor, conductometric measurements were performed with GOD-PAH coated nanoparticles and with directly cross-linked GOD on the conductometric sensor. The relationship between biosensor response and glucose concentration was examined between 0.04 mM and 1 mM range. Fig. 5 shows the calibration curve of the glucose sensor measured under the optimum conditions. A sensitivity of 45 μM/mM is observed in the presence of functionalized AuNPs whereas 31 μM/mM is observed when GOD is directly cross-linked on the conductometric sensor.

The limit of detection (LOD), calculated as three times the signal-to-background ratio by extrapolating the calibration curve linearly below 10^{-4} M, was 50 μM of glucose when GOD is directly deposited on the top of the IDEs and 9 μM when GOD functionalized gold nanoparticles are deposited on the top of the IDEs. A relative standard deviation of 3% was obtained as intra-sensor reproducibility.

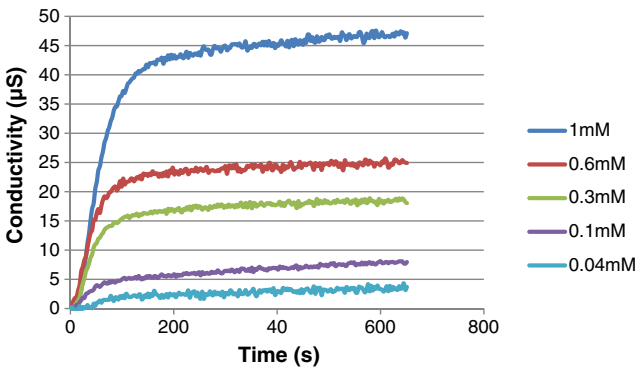

Fig. 4. Evaluation of conductance response of the glucose sensor in the presence of gold nanoparticles (5 mM phosphate buffer, pH = 7.3) for glucose concentrations.

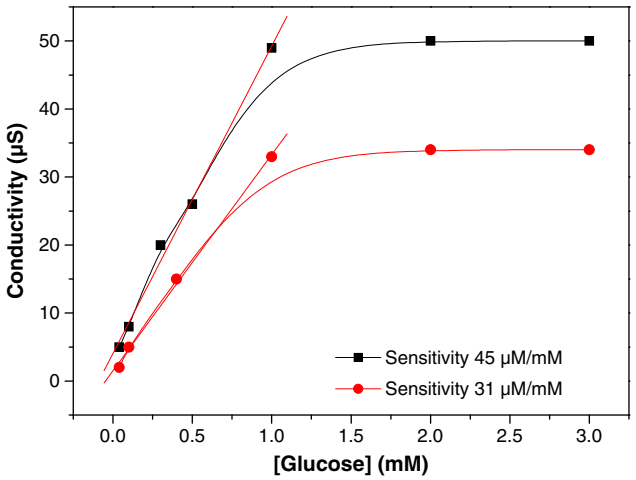

Fig. 5. Calibration curve of glucose sensor (with (black curve) and without (red curve) functionalized gold NPs, 5 mM phosphate buffer, pH = 7.3).

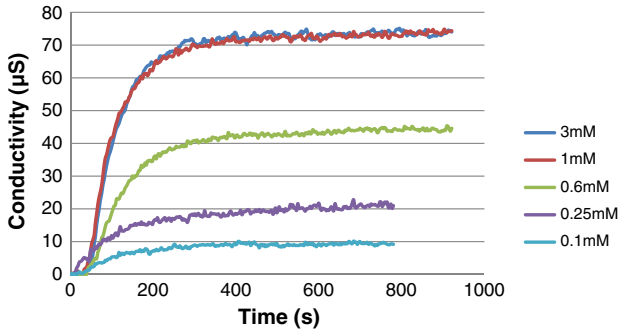

Fig. 6. Evaluation of conductance response of the glucose sensor in the presence of magnetic nanoparticles (5 mM phosphate buffer, pH = 7.3) for glucose concentrations.

3.2.2. Analytical characteristics of glucose conductometric sensor using magnetic nanoparticles (MNPs)

The response kinetics of the conductometric sensor for different concentrations of glucose between 0.1 and 3 mM is shown in Fig. 6. It is clear that when the concentration of glucose increases the amplitude of the response increases too. The response time of the sensor is $\tau_{90} = 4$ min. The calibration curves of glucose sensor without and with functionalized nanoparticles are presented in Fig. 7. The maximum of response obtained with nanoparticles is 75 µS compared to 30 µS for GOD directly cross-linked on the sensor. The dynamic range is from 0.1 mM to 1 mM with GOD-PAH coated MNPs. The limit of detection (LOD), calculated as three times the signal-to-background ratio by extrapolating the calibration curve linearly below 10^{-4} M, is of 3 µM when GOD functionalized MNPs were deposited on the top of the IDEs.

Both methods of enzyme immobilization give lower detection limits than previously reported biosensors [53,54] giving detection limits for glucose of around 20 µM.

The conductometric sensor based on GOD-PAH coated MNPs was stored at 4 °C and was measured every day for 0.6 mM of glucose. As it can be seen in Fig. 8, the biosensor was stable during more than 12 days.

The reproducibility of the biosensor response was tested on five different sensors in PBS solution (5 mM) for 0.6 mM of glucose (Fig. 9). A relative standard deviation of 3% was obtained as intra-sensor reproducibility.

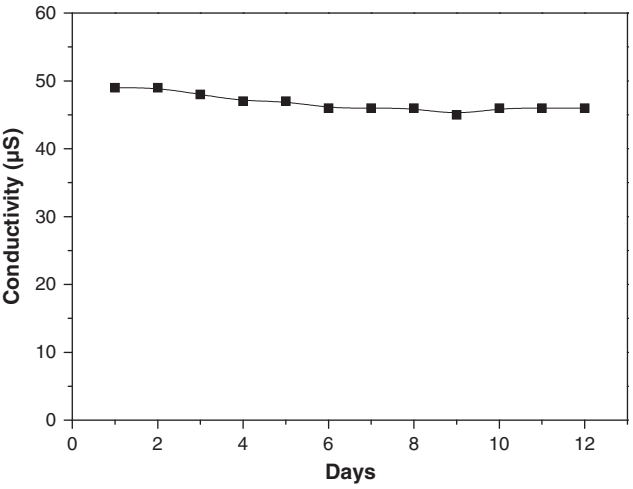

Fig. 8. Study of the GOD/PAH/MNPs storage stability for 0.6 mM of glucose concentration (sensor was stored at 4 °C).

4. Conclusion

In summary, a mediator free biosensor for glucose detection has been fabricated, based on functionalized NPs deposited on an interdigitated conductometric transducer. We have demonstrated that it is possible to improve specifications of the biosensor in comparison to cross-linked GOD biosensor in terms of sensitivity and of detection limit. MNP-based glucose sensors present good stability and good sensor-to-sensor reproductibility. The higher sensitivity was obtained with magnetic nanoparticles which differs from what has been observed for urease biosensors [49,55]. The effect of high conductivity of AuNPs seems not to have any influence of sensitivity of detection with an oxidase enzyme whereas it gives a high amplification in case of hydrolase enzyme. The general character of this observation will be verified and modeled.

One of the key interests of conductometric measurements is that they prevent any Faradaic process, then, in biological application of this type of glucose biosensor, no interference of redox species should be expected.

Supplementary data to this article can be found online at http://dx.doi.org/10.1016/j.msec.2012.08.043.

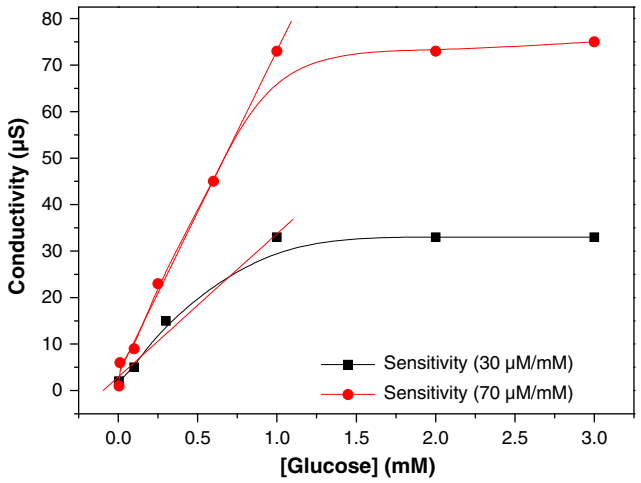

Fig. 7. Calibration curve of glucose sensor (with (red curve) and without (black curve) functionalized gold NPs, 5 mM phosphate buffer, pH = 7.3).

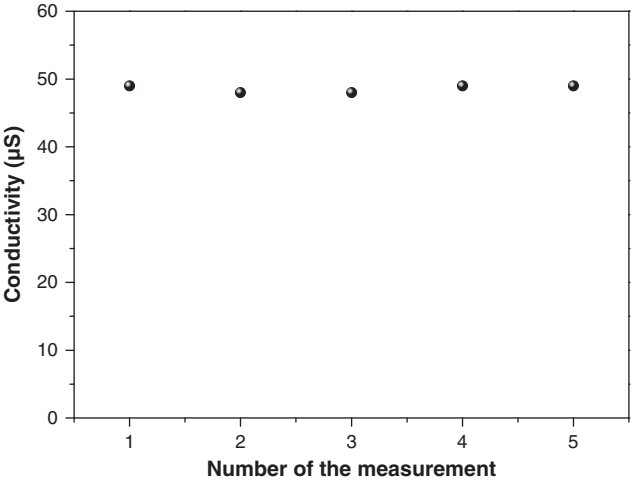

Fig. 9. Study of the reproducibility of the response of the MNP based glucose biosensor for 0.6 mM of glucose concentration.

Acknowledgments

The authors thank EGIDE for the support through UTIQUE programs no. 09G 1128 and no. 10G1103 and through PHC Maghreb No14. W. Nouira thanks the Ministry of Education in Tunisia for the mobility grant. The authors thank the Agence Universitaire de la Francophonie (AUF) for its support through PCSI project no. 6313PS025.

References

[1] H. Luis, J. Alvarez, F. Cervantes, J. Chem. Technol. Biotechnol. 86 (2011) 1354–1363.
[2] G.K. Vertelov, A.Yu. Olenin, G.V. Lisichkin, J. Anal. Chem. 62 (No. 9) (2007) 813–824.
[3] A. Merkoci, FEBS J. 274 (2007) 310–316.
[4] F.S. Ligler, Anal. Chem. 81 (2009) 519–526.
[5] K. Balasubramanian, M. Burghard, Anal. Bioanal. Chem. 385 (2006) 452–468.
[6] O.A. Sadik, A.O. Aluoch, A. Zhou, Biosens. Bioelectron. 24 (2009) 2749–2765.
[7] E. Palecek, M. Fojta, Talanta 74 (2007) 276–290.
[8] I.K. Litos, P.C. Ioannou, T.K. Christopoulos, J. Traeger-Synodinos, E. Kanavakis, Biosens. Bioelectron. 24 (2009) 3135–3139.
[9] J. Hu, P.C. Zheng, J.H. Jiang, G.L. Shen, R.Q. Yu, G.K. Liu, Anal. Chem. 81 (2009) 87–93.
[10] S. Hong, I. Choi, S. Lee, Y.I. Yang, T. Kang, J. Yi, Anal. Chem. 81 (2009) 1378–1382.
[11] Y. Liu, R. Brandon, M. Cate, X. Peng, R. Stony, M. Johnson, Anal. Chem. 79 (2007) 8796–8802.
[12] J. Wang, D. Xu, A. Erdem, R. Polsky, M.A. Salazar, Talanta 56 (2002) 931–938.
[13] E. Palecek, S. Billova, L. Havran, R. Kizek, A. Miculkova, F. Jelen, Talanta 56 (2002) 919–930.
[14] H.B. Fredj, S. Helali, C. Esseghaier, L. Vonna, L. Vidal, A. Abdelghani, Talanta 75 (3) (2008) 740–747.
[15] W.S. Lu, L. Lin, L. Jiang, Biosens. Bioelectron. 22 (2007) 1101–1105.
[16] C.J. Murphy, T. Sau, A. Gole, C. Orendorff, J. Gao, L.F. Gou, S. Hunyadi, T. Li, J. Phys. Chem. B 109 (2005) 13857–13870.
[17] C.J. Murphy, A. Gole, S. Hunyadi, W. Stone, P.N. Sisco, A. Alkiany, B.E. Kinard, P. Hankins, Chem. Commun. 5 (2008) 544–557.
[18] D.X. Li, Q. He, Y. Cui, J.B. Li, Chem. Mater. 19 (2007) 412–417.
[19] M.C. Daniel, D. Astruc, Chem. Rev. 104 (2004) 293–346.
[20] V. Pavlov, Y. Xiao, I. Willner, Nano Lett. 5 (2005) 649–653.
[21] T. Liu, J. Tang, L. Jiang, Biochem. Biophys. Res. Commun. 313 (2004) 3–7.
[22] L. Pasquato, P. Pengo, P. Scrimin, J. Mater. Chem. 14 (2004) 3481–3487.
[23] C. Mateo, J.M. Palomo, G. Fernandez-Lorente, J.M. Guisan, R. Fernandez-Lafuente, Microb. Technol. 40 (2007) 1451–1463.
[24] A. Sassolas, Loïc J. Blum, Béatrice D. Leca-Bouvier, Biotechnol. Adv. 06487 (2011) 22.
[25] I. Willner, B. Basnar, B. Willner, FEBS J. 274 (2007) 302–309.
[26] N. Jaffrezic-Renault, C. Martelet, Y. Chevolot, J.-P. Cloarec, Sensors 7 (2007) 589–614.
[27] S. Zeng, K.T. Yong, I. Roy, X.Q. Dinh, X. Yu, F. Luan, Plasmonics 6 (2011) 491–506.
[28] M.E. Marin-Zamoraa, F. Rojas-Melgarejoa, F. Garcia-Cànovasb, P.A. Garcia-Ruiz, Biotechnology 126 (2006) 295–303.
[29] M. Rebros, M. Rosenberg, Z. Mlichovà, L. Kristofikovà, M. Paluch, J. Enzyme Microb. Technol. 39 (2006) 800–804.
[30] R.J. Jegan, A.T. Emilia, J. Mol. Catal. B: Enzym. 38 (2006) 31–36.
[31] F.J. Xu, Q.J. Cai, Y.L. Li, E.T. Kang, K.G. Neoh, Biomacromolecules 6 (2005) 1012–1020.
[32] N.C.M. Zanon, O.N. Oliveira, L. Caseli, Colloid Interface Sci. 373 (2012) 69–74.
[33] K.H. Wang, M.J. Syu, C.H. Chang, Y.L. Lee, Sens. Actuators B 164 (2012) 29–36.
[34] M. Sari, S. Akgol, M. Karatas, A. Denizli, Ind. Eng. Chem. Res. 45 (2006) 3036–3043.
[35] D. Losic, J.G. Shapter, J.J. Gooding, Langmuir 18 (14) (2002) 5422–5428.
[36] F. Caruso, C. Schuler, Langmuir 16 (24) (2000) 9595–9603.
[37] J.J. Davis, K.S. Coleman, B.R. Azamian, C.B. Bagshaw, M.L.H. Green, J. Chem. Eur. 9 (16) (2003) 3732–3739.
[38] G. Liu, Y. Lin, Electrochem. Commun. 8 (2) (2006) 251–256.
[39] S. Zhang, N. Wang, H. Yu, Y. Niu, C. Sun, Bioelectrochemistry 67 (1) (2005) 15–22.
[40] E.I. Iwuoha, M.R. Smyth, M.E.G. Lyons, Biosens. Bioelectron. 12 (1) (1997) 53–75.
[41] J.J. Mitala Jr., A.C. Michael, Anal. Chim. Acta 556 (2) (2006) 326–332.
[42] D. Shan, Y. He, S. Wang, H. Xue, H. Zheng, Anal. Biochem. 356 (2) (2006) 215–221.
[43] C.Y. Jiang, V.V. Tsukruk, Adv. Mater. 18 (2006) 829–840.
[44] O. Pänke, T. Balkenhohl, J. Kafka, D. Schäfer, F. Lisdat, Adv. Biochem. Eng. Biotechnol. 109 (2008) 195–237.
[45] N.F. Sheppard Jr., D.J. Mears, A. Guiseppi-Elie, Biosens. Bioelectron. 11 (1996) 967–979.
[46] P. Temple-Boyer, A. BenYahia, W. Sant, M.L. Pourciel-Gouzy, J. Launay, A. Martinez, Sens. Actuators B Chem. 131 (2008) 525–532.
[47] A.M. Nyamsi Hendji, N. Jaffrezic-Renault, Claude Martelet, A.A. Shul'ga, S.V. Dzydevich, A.P. Soldatkin, A.V. El'skaya, Sens. Actuators B 21 (1994) 123–129.
[48] A.P. Soldatkin, A.V. El'skaya, A.A. Shul'ga, A.S. Jdanova, S.V. Dzyadevich, N. Jaffrezic-Renault, C. Martelet, P. Clechet, Anal. Chim. Acta 288 (1994) 197–203.
[49] W. Nouira, A. Maaref, F. Vocanson, M. Siadat, J. Saulnier, F. Lagarde, N. Jaffrezic-Renault, Electroanalysis 24 (2012) 1088–1094.
[50] M. Souiri, L. Mora-Ponsonnet, K. Glinel, A. Othmane, T. Jouenne, A.C. Duncan, Colloids Surf., B 68 (2009) 125–129.
[51] N. Jaffrezic-Renault, S.V. Dzyadevych, Sensors 8 (2008) 2569–2588.
[52] A. Sze, D. Erickson, Ren Li, D. Li, Colloid Interface Sci. 261 (2003) 402–410.
[53] S. Zhang, N. Wang, Y. Niu, C. Sun, Sens. Actuators B 109 (2005) 367–374.
[54] M.M. Barsan, C.M.A. Brett, Bioelectrochemistry 76 (2009) 135–140.
[55] W. Nouira, A. Maaref, M. Siadat, A. Errachid, N. Jaffrezic-Renault, Sens. Lett. 9 (2011) 2272–2274.